A monolithic approach to thermo-structure interaction in rocket nozzles

Caroline Danowski⋆*, Volker Gravemeier*⋆,⋆⋆*, Ulrich Küttler*⋆*, Michael W. Gee*⋆⋆⋆ *and Wolfgang A. Wall*⋆
⋆*Institute for Computational Mechanics*
⋆⋆*Emmy Noether Research Group "Computational Multiscale Methods for Turbulent Combustion"*
⋆⋆⋆*Mechanics and High Performance Computing Group*
Technische Universität München
Boltzmannstraße 15, D-85747 Garching, Germany

Abstract

In the present work, a monolithic solution approach based on a finite element method for the problem of thermo-structure interaction (TSI) in the challenging field of rocket nozzles is proposed, with independently discretised structural and thermal fields. For the monolithic TSI scheme, an iterative solver (GMRES) and a Block-Gauss-Seidel preconditioner is used. The proposed methods are tested for the second Danilovskaya problem, and good agreement of the numerical results with results from the literature is observed. Furthermore, it is shown that the monolithic algorithm exhibits improved stability compared to partitioned algorithms.

1. Introduction

Better understanding of complex thermo-fluid-structure interaction (TFSI) is essential for the design of rocket nozzles. One important ingredient for such investigations is an efficient and robust computational approach for the analysis of thermo-structure-coupled dynamics. Challenging features of this problem type can be demonstrated with the help of Fig.1, which shows the combustion chamber of the Ariane 5 main engine "Vulcain". Elevated temperatures (combustion temperature up to 3600 K) with high temperature gradients (coolant fluid inlet temperature approximately 73 K), high wall heat fluxes (of about 120 MW/m^2), high-geometrical non-linearities due to very thin structure, high Mach- and Reynolds-numbers, and complex shock-boundary-layer interaction have to be considered. Experiments investigating important phenomena of a nozzle are extremely difficult, because the actual test environment is located on earth and in space. Due to extrem material loading, the so-called dog-house effect occurs, cf. Fig. 2. The dog-house effect or

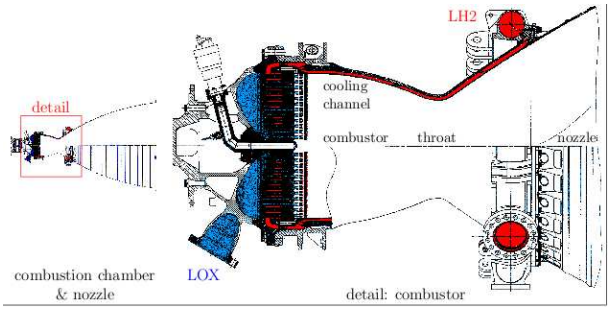

Figure 1: Engineering drawing of the combustion chamber of the Ariane 5 main engine "Vulcain" (cf. [13])

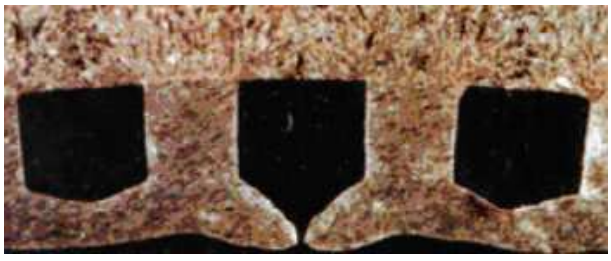

Figure 2: Detailed cross-section at the inner radius of the thrust cell linear showing the failure site in the center cooland channel (cf. [4])

failure is a complex cracking phenomenon likely caused by cyclic loading, creep and chemical damage. Control loss and therefore failure of an Ariane 5 ECA in the year 2002 is said to be related to the dog-house effect.

To understand this effect and to optimize current rocket nozzles, our work presented in the following aims at developing an adequate computational approach. As starting point for the complete TFSI model, we present a

submodel capable of describing thermo-structure interactions for the application to rocket nozzles. Both partitioned and monolithic coupling algorithms for TSI are basically possible. In partitioned schemes, loosely ("one-way staggered") and strongly ("iterative staggered") coupled algorithms are differentiated. One-way staggered schemes accept that the coupling condition is not fulfilled exactly at the end of a time step. In contrast, iterative staggered schemes aim at achieving equilibrium of the overall system of equations at the end of a time step through iterations between the partitioned fields. However, recent literature such as [7, 10] pointed out that well-designed monolithic algorithms are even superior to accelerated iterative staggered schemes. An essential aspect for an efficient solution, especially for large-scale problems, is a good preconditioning technique. Various preconditioners based on algebraic multigrid (AMG) methods were proposed in [7, 10] for monolithic solution schemes of coupled problems, such as fluid-structure interaction (FSI). If properly designed, they were shown to enable a fast, efficient, and robust solution of the overall fully-coupled problem.

The main focus of this paper is on a new monolithic scheme using an Block-Gauss-Seidel preconditioner for the nonsymmetric system of TSI. The long-term perspective of this project is to fully couple the presented TSI model to a Large eddy simulation (LES) approach to turbulent flow, including shock-boundary-layer interactions. The complete model should reproduce all working stages of a rocket nozzle. To the best of the authors' knowledge, there has not yet been any computational model proposed capable of addressing all aforementioned features for a rocket nozzle. Since no experimental validation will be possible for the target system, it is essential to compose the simulation approach of well-validated, reliable, effective and robust building blocks, such as the TSI model sketched here.

2. Problem definition

For the description of deformation in rocket nozzles due to hot gases, the displacement field and the temperature field are considered. The resulting thermomechanical system is a fully-coupled problem, that is, the solution of the temperature field depends on the displacement field and vice versa. The coupling of the two fields in TSI is determined by its material. On the one hand, the material is able to display stress changes due to temperature changes. On the other hand, temperature changes due to mechanical heating can be demonstrated.

In the following it is focused on thermoelastic material. Moreover, thermomechanical influences in both directions (i.e., the influence of temperature on the mechanical side as well as the influence of deformation on the thermal side) are considered. Non-linear thermo-elastic material effects are neglected.

2.1 Structural field equations

In this work we assume a structural field governed by the linear elastodynamic equation

$$\rho\,\ddot{\boldsymbol{u}} \;=\; \nabla\cdot\boldsymbol{\sigma} \;+\; \hat{\boldsymbol{b}} \tag{1}$$

that describes equilibrium between the forces of inertia, internal and external force $\hat{\boldsymbol{b}}$ in the undeformed structural configuration Ω. Equation (1) has to be solved for the unknown displacements $\boldsymbol{u}$. The internal forces are expressed in terms of the stress tensor $\boldsymbol{\sigma}$. To describe the stress, a constitutive strain-energy ψ law has to be considered. The stress equation can be derived using (3) by the definition:

$$\boldsymbol{\sigma} \;=\; \rho\frac{\partial\psi}{\partial\boldsymbol{\varepsilon}} \tag{2}$$

including the linear strain tensor (5). For an isotropic thermoelastic solid, the strain energy function described in the free Helmholtz energy ψ follows as

$$\rho\,\psi(\boldsymbol{\varepsilon},T) \;=\; \mu\,\boldsymbol{\varepsilon}\cdot\boldsymbol{\varepsilon} \;+\; \frac{1}{2}\lambda(\boldsymbol{\varepsilon}\cdot\mathbf{1})^2 \;+\; m\,\Delta T\,\boldsymbol{\varepsilon}\cdot\mathbf{1} \;-\; \rho\,C_{\mathrm{V}}(T\ln\frac{T}{T_0} \;-\; \Delta T)\,. \tag{3}$$

The stress equation results in

$$\boldsymbol{\sigma} \;=\; 2\,\mu\,\boldsymbol{\varepsilon} \;+\; \lambda\,(\boldsymbol{\varepsilon}\cdot\mathbf{1})\,\mathbf{1} \;+\; m\,\Delta T\,\mathbf{1} \tag{4}$$

with the stress-temperature modulus $m \;=\; -(2\,\mu + 3\,\lambda)\,\alpha_{\mathrm{T}}$, including the Lamé-constants λ,μ, and the coefficient of thermal expansion α_{T}. The temperature difference ΔT is defined as the difference between the current temperature T

and the initial temperature T_0 at $t = 0$: $\Delta T = T - T_0$. Small strains are assumed, so that higher-order terms can be neglected, such that:

$$\boldsymbol{\varepsilon} = \frac{1}{2}(\nabla_0 \boldsymbol{u} + \nabla_0^{\mathrm{T}} \boldsymbol{u}) = \frac{1}{2}(\nabla \boldsymbol{u} + (\nabla \boldsymbol{u})^{\mathrm{T}}) \quad , \quad \dot{\boldsymbol{\varepsilon}} = \frac{1}{2}(\nabla_0 \dot{\boldsymbol{u}} + \nabla_0^{\mathrm{T}} \dot{\boldsymbol{u}}) = \frac{1}{2}(\nabla \dot{\boldsymbol{u}} + (\nabla \dot{\boldsymbol{u}})^{\mathrm{T}}) \,, \tag{5}$$

with the infinitesimal strain tensor $\boldsymbol{\varepsilon}$ and the resulting strain rate tensor $\dot{\boldsymbol{\varepsilon}}$. Appropriate boundary and initial conditions have to be defined for the structural field as well. If the material can be understood as a potential, i.e. the internal work is independent of the path and no friction is considered, then the weak form can be interpreted as variation of an energy potential. In the context of energy potential the test function is interpreted as virtual displacement, and (1) is weighted by virtual displacemts $\delta \boldsymbol{d}$ and then integrated by parts:

$$\int_\Omega \rho \, \ddot{\boldsymbol{u}} \cdot \delta \boldsymbol{d} \, \mathrm{d}\Omega + \int_\Omega \boldsymbol{\sigma} \cdot \nabla \delta \boldsymbol{d} \, \mathrm{d}\Omega - \int_\Omega \hat{\boldsymbol{b}} \cdot \delta \boldsymbol{d} \, \mathrm{d}\Omega - \int_{\Gamma_t} \hat{\boldsymbol{t}} \cdot \delta \boldsymbol{d} \, \mathrm{d}\Gamma = \boldsymbol{0} \tag{6}$$

Equation (6) describes the partial, weak structural balance of equation including the traction vector $\hat{\boldsymbol{t}} := \boldsymbol{\sigma} \cdot \boldsymbol{n}$. The structural field equation is discretised in space with a finite element method (FEM). For details about the FEM for the structural field the reader is referred to the respective literature, e.g., [9, **?**]. For temporal discretisation, we use a one-step-θ time-integration scheme.

2.2 Thermal field equations

Assuming validity of first and second law of thermodynamics and integration of the strain-energy potential (3), we obtain

$$\rho C_{\mathrm{V}} \dot{T} - T m \mathbf{1} : \dot{\boldsymbol{\varepsilon}} + \nabla \cdot \boldsymbol{q} - \rho r = 0 \tag{7}$$

as the equation for the temperature evolution. r in (7) defines the radiation. In all further investigations, we neglect the radiation r. A constitutive law has to be chosen to determine the heat flux $\boldsymbol{q}$. Fourier's law, which is linear and isotropic, is defined as

$$\boldsymbol{q} = -k \nabla T \,, \tag{8}$$

with the thermal conductivity k, which is assumed constant and positive.

Appropriate boundary and initial conditions for the temperature field have to be chosen as well. Similarly to the structural field, a weak form of the thermal equation (7) is obtained. The test function is here interpreted as virtual temperatures. Weighted by virtual temperatures δT and then integrated by parts, (7) results in:

$$\int_\Omega \rho C_{\mathrm{V}} \dot{T} \, \delta T \, \mathrm{d}\Omega - \int_\Omega T m \mathbf{1} : \dot{\boldsymbol{\varepsilon}} \, \delta T \, \mathrm{d}\Omega - \int_\Omega \boldsymbol{q} \cdot \nabla \delta T \, \mathrm{d}\Omega - \int_\Gamma \bar{q} \, \delta T \, \mathrm{d}\Gamma = 0 \,. \tag{9}$$

For the thermal field, due to *Newton's law of heat dissipation*, heat convection boundary conditions can be specified on the boundary Γ_c as follows:

$$-\boldsymbol{q} \cdot \boldsymbol{n} = -(-k \nabla T) \cdot \boldsymbol{n} =: \bar{q}_c = h (T - T_\infty) \quad \text{on} \, \Gamma_c \, [\times (0, t_{\mathrm{end}})] \tag{10}$$

with linear heat transfer coefficient h, and the ambient temperature T_∞. Heat convection boundary conditions represent non-linear von Neumann boundary conditions for the temperature field. Due to the non-linearities this boundary condition has to be considered in the linearisation as well.

In accordance with the structural field the thermal field is also discretised in space with the FEM and temporally discretised with a one-step-θ time-integration scheme.

3. Monolithic solution approach

In a monolithic algorithm the fully-coupled nonlinear TSI system

$$\boldsymbol{K}_{\mathrm{TSI}}^{i+1} \Delta \boldsymbol{x}_{n+1}^{i+1} = -\boldsymbol{f}_{\mathrm{TSI},n+1}^{i+1} \tag{11}$$

is solved for the time step t_{n+1} and the (Newton) iteration-step $i + 1$. All degrees of freedom of the TSI-system $\Delta \boldsymbol{x}_{n+1}^{i+1}$, i.e., the displacement and the temperature increments, are calculated simultaneously. Monolithic algorithms require a

complete linearisation of the problem. A challenge in TSI is the non-symmetric tangent matrix $\boldsymbol{K}_{\mathrm{TSI}}$. The TSI matrix is given as follows:

$$\underbrace{\begin{bmatrix} \boldsymbol{K}_{\boldsymbol{uu}} & \boldsymbol{K}_{\boldsymbol{u}\theta} \\ \boldsymbol{K}_{\theta\boldsymbol{u}} & \boldsymbol{K}_{\theta\theta} \end{bmatrix}}_{\boldsymbol{K}_{\mathrm{TSI}}^{i+1}} \underbrace{\begin{bmatrix} \Delta \boldsymbol{d}_{n+1}^{i+1} \\ \Delta \boldsymbol{T}_{n+1}^{i+1} \end{bmatrix}}_{\Delta \boldsymbol{x}_{n+1}^{i+1}} = \underbrace{\begin{bmatrix} -\boldsymbol{\mathcal{F}}_{m,n+1}^{i+1} \\ -\boldsymbol{\mathcal{F}}_{t,n+1}^{i+1} \end{bmatrix}}_{-\boldsymbol{\mathcal{F}}_{n+1}^{i+1}} \tag{12}$$

where the residual $\boldsymbol{\mathcal{F}}_m$ describes the structural equation (6) and $\boldsymbol{\mathcal{F}}_t$ the thermal equation (9). The tangent matrix $\boldsymbol{K}_{\mathrm{TSI}}$ can be split in four parts, as shown in (12):

$$\boldsymbol{K}_{\boldsymbol{uu}} = \bigA_{e=1}^{nele} \Big[\int_{\Omega^{(e)}} \boldsymbol{B}_{\boldsymbol{u}}^{\mathrm{T}} \boldsymbol{C}\, \boldsymbol{B}_{\boldsymbol{u}} \mathrm{d}\Omega + \frac{1}{\theta \Delta t^2} \int_{\Omega^e} \boldsymbol{N}_{\boldsymbol{u}}^T \rho\, \boldsymbol{N}_{\boldsymbol{u}}\, \mathrm{d}\Omega \Big]^{(e)}, \tag{13}$$

$$\boldsymbol{K}_{\theta\theta} = \bigA_{e=1}^{nele} \Big[\frac{1}{\theta \Delta t} \int_{\Omega^{(e)}} \boldsymbol{N}_\theta^T \left(\rho\, C_{\mathrm{V}}\right) \boldsymbol{N}_\theta \, \mathrm{d}\Omega + \int_{\Omega^{(e)}} \boldsymbol{B}_\theta^{\mathrm{T}}\, k\, \boldsymbol{B}_\theta \, \mathrm{d}\Omega - \int_{\Gamma^{(e)}} \boldsymbol{N}_\theta^T\, h\, \boldsymbol{N}_\theta \, \mathrm{d}\Gamma_c - \int_{\Omega^{(e)}} \boldsymbol{N}_\theta^T\, \boldsymbol{C}_\theta : \boldsymbol{B}_{\boldsymbol{u}}\, \dot{\boldsymbol{d}}\, \boldsymbol{N}_\theta \, \mathrm{d}\Omega \Big]^{(e)}, \tag{14}$$

$$\boldsymbol{K}_{\boldsymbol{u}\theta} = \bigA_{e=1}^{nele} \Big[\int_{\Omega^{(e)}} \boldsymbol{B}_{\boldsymbol{u}}^T\, m\, \boldsymbol{I}\, \boldsymbol{N}_\theta \, \mathrm{d}\Omega \Big]^{(e)} = \bigA_{e=1}^{nele} \Big[\int_{\Omega^{(e)}} \boldsymbol{B}_{\boldsymbol{u}}^T\, \boldsymbol{C}_\theta\, \boldsymbol{N}_\theta \, \mathrm{d}\Omega \Big]^{(e)}, \tag{15}$$

$$\boldsymbol{K}_{\theta\boldsymbol{u}} = \bigA_{e=1}^{nele} \Big[-\frac{1}{\theta \Delta t} \int_{\Omega^{(e)}} \boldsymbol{N}_\theta^T\, \boldsymbol{N}_\theta \boldsymbol{T}\, \boldsymbol{C}_\theta \, \mathrm{d}V \Big]^{(e)} \quad . \tag{16}$$

$\boldsymbol{K}_{\boldsymbol{uu}}$ (13) represents the purely mechanical tangent, $\boldsymbol{K}_{\theta\theta}$ (14) the purely thermal tangent. The off-diagonal terms emerge by the strong coupling effects in TSI: $\boldsymbol{K}_{\boldsymbol{u}\theta}$ (15) describes the mechanical-thermal tangent, and finally $\boldsymbol{K}_{\theta\boldsymbol{u}}$ (16) the thermal-mechanical tangent.

Large linear systems of equations cannot be solved effectively with a direct solver often iterative Krylov methods are applied (see, e.g., [15, 11]). For a detailed description of iterative Krylov methods the interested reader is directed to these publications. Furthermore, the properties of the structure and temperature submatrices in the monolithic TSI system of equations (12) differ considerably. As a consequence, standard preconditioners cannot be applied adequately. Alternatively, block preconditioners, for instance block-Gauss-Seidel (BGS) and algebraic multigrid (AMG) block precondtioners, were proposed in [7, 10] for FSI problems. A similar approach with BGS preconditioner is used here and described in the following.

A right preconditioner (identifier R in (17)) implies the introduction of an invertible preconditioner matrix $\boldsymbol{M}_{\mathrm{R}}$ into (11):

$$\boldsymbol{K}_{\mathrm{TSI}} \boldsymbol{M}_{\mathrm{R}}^{-1} \underbrace{\boldsymbol{M}_{\mathrm{R}}\, \boldsymbol{x}_{i+1}}_{:=\bar{\boldsymbol{x}}} = \boldsymbol{f}_{\mathrm{TSI}}\,. \tag{17}$$

For effective preconditioning, the preconditioner matrix $\boldsymbol{M}_{\mathrm{R}}$ should approximate the stiffness matrix of the coupled TSI system (or Jacobian of the TSI problem): $\boldsymbol{M}_{\mathrm{R}} \approx \boldsymbol{K}_{\mathrm{TSI}}$. A Krylov solver relies on a repeated matrix-vector product. $\boldsymbol{x}_{i+1} = \boldsymbol{M}_{\mathrm{R}}^{-1}\, \bar{\boldsymbol{x}}_{i+1}$ to get the exact solution $\boldsymbol{x}_{i+1}$ using the inverse of the preconditioner matrix. Hence, $\boldsymbol{M}_{\mathrm{R}}$ should be easily invertible for an efficient solution process. To start the iteration, an initial guess for $\bar{\boldsymbol{x}}_0$ is needed.

$$\underbrace{\begin{bmatrix} \boldsymbol{K}_{\mathrm{SS}}^i & \boldsymbol{K}_{\mathrm{ST}}^i \\ \boldsymbol{K}_{\mathrm{TS}}^i & \boldsymbol{K}_{\mathrm{TT}}^i \end{bmatrix}}_{\boldsymbol{K}_{\mathrm{TSI}}} \underbrace{\begin{bmatrix} \Delta \boldsymbol{d}_i^{n+1} \\ \Delta T_i^{n+1} \end{bmatrix}}_{\Delta \boldsymbol{x}} = -\underbrace{\begin{bmatrix} \boldsymbol{r}_i^{\boldsymbol{d},n+1} \\ \boldsymbol{r}_i^{T,n+1} \end{bmatrix}}_{\boldsymbol{f}^{\mathrm{TSI}}} \tag{18}$$

For the TSI system, two block equations must be solved for the preconditioner. As in [11, 7] for FSI, we solve the block equations successively for the presented TSI system. In FSI, the structural solution directly influences the fluid solution, whereas the fluid solution influences the structural solution not until the next iteration step. This is due to the fact that the effect of the deformation on the flow is usually stronger than the effect of the fluid on the deformation. In TSI, the effect of the structural field on the thermal field is less important than the opposite effect. In fact, the heating due to elastic deformation (i.e., the influence of the structural on the thermal field is often neglected, see e.g., [12, 13, 2]). Especially if an elastic material law is assumed, the thermoelastic heating term is only significant if dissipation is considered. Otherwise, it is rather small, such that its neglection is a valid assumption.
For solving the TSI system, we start by solving the thermal equation using the displacements resulting from the previous

Block-Gauss-Seidel iteration step j. The resulting temperatures T_{j+1} are used for calculating the new displacements $\boldsymbol{d}_{j+1}$.

$$\boldsymbol{K}^i_{\mathrm{TT}}\,\Delta\boldsymbol{T}^{n+1}_{i,j+1} \;=\; \boldsymbol{r}^{T,n+1}_i - \boldsymbol{K}^i_{\mathrm{TS}}\,\Delta\boldsymbol{d}^{n+1}_{i,j}\,, \quad \boldsymbol{K}^i_{\mathrm{SS}}\,\Delta\boldsymbol{d}^{n+1}_{i,j+1} \;=\; \boldsymbol{r}^{\boldsymbol{d},n+1}_i - \boldsymbol{K}^i_{\mathrm{ST}}\,\Delta T^{n+1}_{i,j+1} \tag{19}$$

As abort criterion for the Block-Gauss-Seidel iteration, we require the following two conditions to be fulfilled:

$$|\Delta\boldsymbol{d}^{n+1}_{i,j+1} \;-\; \Delta\boldsymbol{d}^{n+1}_{i,j}| \leq\; \varepsilon^S\,, \quad |\Delta T^{n+1}_{i,j+1} \;-\; \Delta T^{n+1}_{i,j}| \leq\; \varepsilon^T\,, \tag{20}$$

with a given tolerance ε^S for the displacement increment $\Delta\boldsymbol{d}$ as well as ε^T for the temperature increment ΔT.

To validate the present monolithic TSI approach, we compare the results with a fully-coupled partitioned TSI algorithm. Literature research has shown, that a thermo-structure interaction problem is usual solved with a partitioned scheme, cf. [5, 1, 14, 8, 12, 13, 2].

4. Numerical Examples

The second Danilovskaya problem as proposed in [3], which has often been used in literature for validation of a fully-coupled thermomechancial model (e.g., in [5, 18, 16, 17]) is considered. The problem is essentially one-dimensional. A linear elastic half-space ($x > 0$) is subjected to a uniform sudden temperature change due to a heat flux q_c on the surface $x = 0$ according to (10). The actual geometry in the form of a cuboid of height and width of 4 mm and a length of 6 mm is shown in Fig. 3. The second Danilovskaya model as considered in [3, 5, 17] includes the assumption that

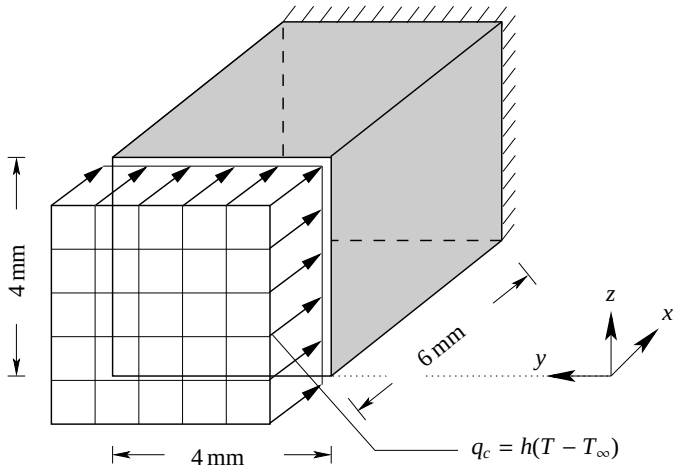

Figure 3: Initial geometry and heat flux

the thermomechanical coupling term in the energy balance equation (7) does not include the absolute temperature T but the initial temperature T_0. This simplifies the thermal subproblem, because the linearisation of this term with respect to T can be neglected. The second term in (7) reduces to $-\,T_0\,m\,\mathbf{1} : \dot{\boldsymbol{\varepsilon}}$, so that

$$\rho\,C_{\mathrm{V}}\,\dot{T} \;-\; T_0\,m\,\mathbf{1} : \dot{\boldsymbol{\varepsilon}} \;+\; \nabla\cdot\,\boldsymbol{q} \;-\; \rho\,r \;=\; 0\,. \tag{21}$$

Hence, the coupling term is independent of the absolute temperature solution and therefore can be interpreted as an external load. The simulation is carried out in three spatial dimensions, fixing all displacement degrees of freedom in y- and z-direction, such that only uniaxial (quasi-one-dimensional) motion is enabled. The body is assumed to be mechanically constrained and thermally insulated. The initial and boundary conditions are given as

$$u_x(x, t=0) = 0 = \dot{u}_x(x, t=0), \quad T(x, t=0) = T_0, \quad \text{and} \quad \hat{t}_i(x=0, t) = 0\,. \tag{22}$$

The thermal field properties are given by the thermal diffusivity $k \;=\; 1.03{\times}10^3\,\mathrm{mm^2\,kg/(s^3\,K)}$, the linear heat expansion coefficient $\alpha_{\mathrm{T}} \;=\; 1.1{\times}10^{-5}\,1/\mathrm{K}$ and the kinematic heat transfer coefficient $\bar{h} = 0.1\,\mathrm{mm/s}$ (defined as $\bar{h} \;=\; h/(\rho\,C_{\mathrm{V}})$ with the linear heat transfer coefficient h, cf. (10)), a constant initial temperature $T_0 \;=\; 273.15\,\mathrm{K}$, an ambient temperature $T_\infty \;=\; 373.15\,\mathrm{K}$ as well as the specific heat capacity $C_{\mathrm{V}} \;=\; 8.21 \times 10^6\,\mathrm{mm^2/(s^2\,K)}$. For the structural field, a Young's

modulus $E = 210\,\text{GPa}$, a Poisson's rate $\nu = 0.3$ and a density $\rho = 7.85 \times 10^{-6}\,\text{kg/mm}^3$ are chosen. The structural and the thermal field are both discretised with $12 \times 4 \times 4$ hexahedral elements. The simulation time is $t = 4\,\text{s}$, with a time-step size of $\Delta t = 0.001\,s$. Heat-convection boundary conditions are used at the surface $x = 0$. A linear thermoelastic material is chosen, according to equation (4).

Displacements and temperatures are evaluated at the centre point of plane $x = 1\,\text{mm}$. The value θ for time-integration is set to be 0.5. The present results are compared to the ones in [17]. Unfortunately, not all material

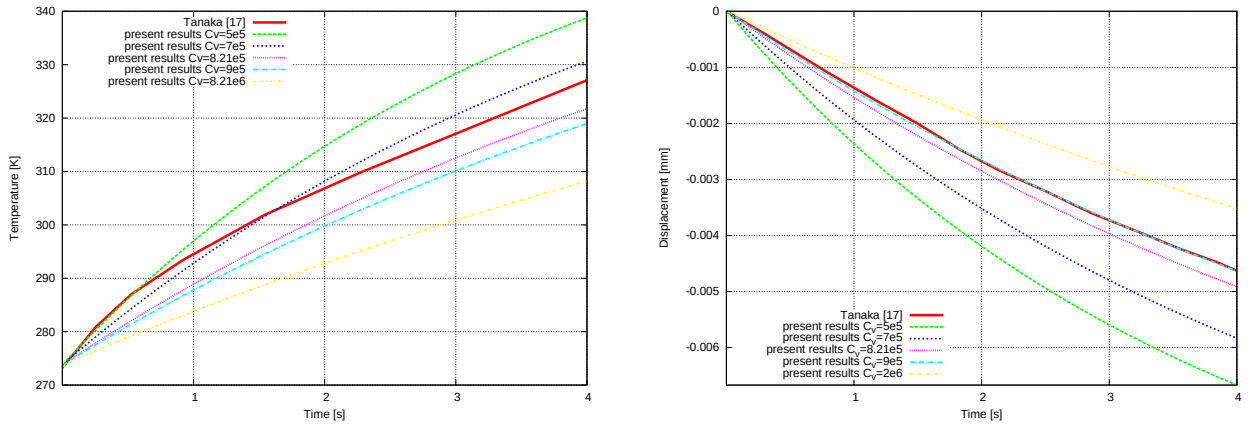

Figure 4: Temperature (left) and displacement (right) results.

parameters for the second Danilovskaya problem are specified in [5, 18, 16, 17]: dependent on the dimensionless thermomechanical coupling parameter δ introduced in [5, 1, 17], the density ρ and the heat capacity C_V can be chosen arbitrarily. Fig. 4 depicts the spread of the results for temperature and displacements in x-direction depending on a variation of the values for C_V, using an iterative staggered partitioned TSI algorithm.

The proposed monolithic TSI algorithm is now compared to the fully-coupled partitioned iterative staggered algorithm with mechanical predictor. In contrast to the simplifying assumption in [5, 18, 16, 17] (equation (21)), in the following, the absolute temperature as given in (7) will be taken into account. Due to that, an additional reactive term, which is well-known for being a potential source of numerical stability problems, appears in comparison to the parabolic partial differential equation (21).

However, even with the inclusion of the reactive term, the monolithic TSI algorithm converges for various choices of material parameters, including the present one. As expected, the results obtained for the thermal equation incorporating the absolute temperature differ from the results obtained for the simplified thermal equation: Fig. 5 shows the results ("monolithic") compared to the results for the simplified thermal equation ("T_0 partitioned"): a notably smaller increase and decrease for the temperatures and the displacements, respectively, is observed. Severe problems occur for the iterative staggered partitioned TSI algorithm with mechanical predictor in the form of oscillations and bad convergence for the given material parameters.

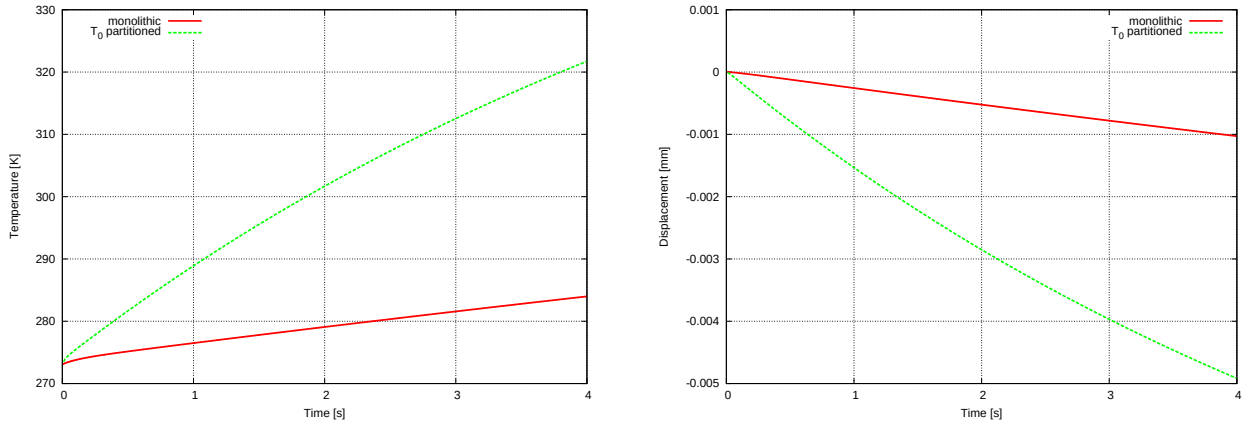

Figure 5: Temperature (left) and displacement (right) results .

The Young's modulus is identified as a parameter influencing this observed behaviour. In Fig. 6, exemplary results for temperature and displacement are provided respectively, when reducing the modulus by a factor of 100. In this case, stable results can again be obtained using a partitioned algorithm for this reduced Young's modulus. The results obtained with the monolithic TSI algorithm for both values of Young's modulus are shown as well as the results obtained with the partitioned algorithm. For the reduced modulus, the results are in good agreement.

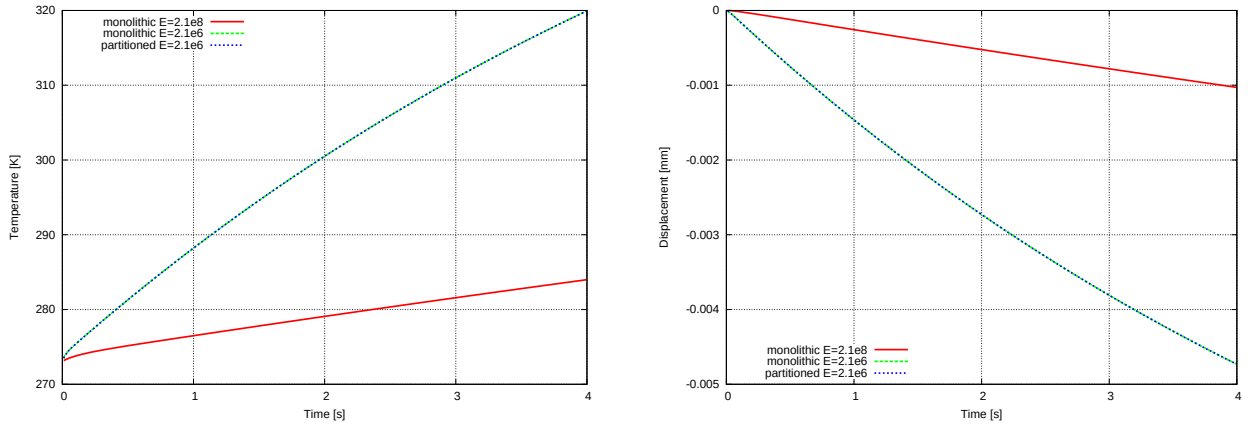

Figure 6: Temperature (left) and displacement (right) results varying E-modulus.

5. Concluding Remarks

A monolithic algorithm for thermo-structure interaction problems has been presented. Validation of the algorithm has been done for a numerical example in the form of the second Danilovskaya problem, comparing the results to results obtained with partitioned algorithms previously proposed in literature. In contrast to those earlier approaches in literature, the proposed thermo-structure interaction formulation enables for taking the absolute temperature into account in the thermomechanical coupling term of the energy balance. A novel monolithic Newton-Krylov approach with a standard block-Gauss-Seidel preconditioner represents the key part of the proposed method. For the presented numerical example, the monolithic scheme shows improved stability compared to the partitioned scheme. The present work represents a starting point for further studying the challenging problem of thermo-structure interaction. In particular, future work will concern the inclusion of different nonlinear material models into the thermomechanical framework, capable of representing irreversible deformations and dissipation.

6. Acknowledgements

The first author (C. D.) gratefully acknowledges support by the German Research Foundation (Deutsche Forschungsgemeinschaft - DFG) in the framework of the Sonderforschungsbereich Transregio 40 and by the Graduate School of Technische Universität München. The support of the second author (V.G.) via the Emmy Noether Program of the DFG is also gratefully acknowledged.

References

[1] Armero, F., J.C. Simo. 1992. A new unconditionally stable fractional step method for nonlinear coupled thermomechanical problems. *Int. J. Numer. Methods Eng.* 35:737–766

[2] Bornemann, P.B., W.A. Wall. 2007. Thermo-structure-coupled dynamics of thin-walled structures at elevated temperatures. *ECCOMAS Thematic Conference on Computational Methods in Structural Dynamics and Earthquake Engineering. Rethymno, Crete, Greece, 13–16 June 2007*.

[3] Danilovskaya, V.I. 1952. On a dynamical problem of thermoelasticity. *Prikl. Mat. Mekh. 16: 341–344*.

[4] Ellis, D.L., Yun H.M. 1999. Cu-8 Cr-4 Nb alloy for reusable launch vehicle combustion chamber liners. *Insights in R & T Presentation April 13,1999.*

[5] Farhat, C., K.C. Park, Y. Dubois-Pelerin. 1991. An unconditionally stable staggered algorithm for the transient finite-element analysis of coupled thermoelastic problems. *Comput. Methods Appl. Mech. Engrg.* 85:349–365.

[6] Glaser, S. 1998. Gekoppelte thermomechanische Berechnung dünnwandiger Strukturen mit der Methode der Finiten Elemente. *Habilitation Thesis, Institut für Statik und Dynamik der Luft- und Raumfahrtkonstruktionen, Universität Stuttgart*.

[7] Gee, M.W., U. Küttler and W.A. Wall. 2010. Truly monolithic algebraic multigrid for fluid-structure interaction. *Internat. J. Numer. Methods Engrg. in press, available online: Doi: 10.1002/nme.3001*.

[8] Holzapfel, G.A., J.C. Simo. 1996. Entropy elasticity of isotropic rubber-like solids at finite Strains. *Comput. Methods Appl. Mech. Engrg.* 132:17–44.

[9] Hughes, T.J.R. 2000. The Finite Element Method - linear static and dynamic finite element analysis. *Dover Publications, New York, USA.*

[10] Klöppel, T., A. Popp, U. Küttler, and W.A. Wall. 2011. Fluid-structure interaction for non-conforming interfaces based on a dual mortar formulation. *Comp. Meth. in Appl. Mech. and Engng., in press.*

[11] Küttler, U., W.A. Wall. 2009. Vector extrapolation for strong coupling fluid-structure interaction solvers *J. Appl. Mech.* 76.

[12] Kuhl, D. 2002, J. Riccius, O.J. Haidn. Thermomechanical analysis and optimization of cryogenic liquid rocket engines. *J. Propul. Power.* 18: 835–846.

[13] Kuhl, D. 2004. Thermomechanical analysis using finite element methods with particular emphasis on rocket combustion chambers. *ECCOMAS 2004, Jyväskylä, 24–28 July 2004*.

[14] Miehe, C. 1995. Entropic thermoelasticity at finite strains. aspects of the formulation and numerical implementation. *Comput. Methods Appl. Mech. Engrg.* 120: 243–269.

[15] Saad, Y. 2003. Iterative methods for sparse linear systems. *SIAM, Philadelphia, USA.*

[16] Tamma, K.K., R.R. Namburu. 1992. An effective finite element modeling/analysis approach for dynamic thermoelasticity due to second sound effects. *Comput. Mech.* 9:73–84.

[17] Tanaka, M., T. Matsumoto, M. Moradi. 1995. Application of boundary element method to 3-D problems of coupled thermoelasticity. *Eng. Anal. Bound. Elem.* 16:297–303.

[18] Tosaka, N., I.G. Suh. 1991. Boundary element analysis of dynamic coupled thermoelasticity problems. *Comput. Mech.* 8:331–342.

[19] Zienkiewicz, O., Taylor, R.L. 2000. The Finite Element Method Volumes 2 - Solid Mechanics *Butterworth Heinemann*.